[Article ID] 1003- 6326(2001)05- 0675- 06

Diffusive healing of internal fatigue micro-cracks in pure titanium①

YANG Jun-gang(杨君刚)[1,2], SUN Jun(孙 军)[1], ZHANG Hai-long(张海龙)[1]
(1. State Key Laboratory for Mechanical Behavior of Materials, School of Materials Science and Engineering, Xi'an Jiaotong University, Xi'an 710049, P. R. China;
2. School of Materials Science and Engineering, Xi'an University of Technology, Xi'an 710048, P. R. China)

[Abstract] The internal micro-cracks with the critical length about 30 μm and thickness less than 1 μm were introduced into the pure titanium samples by uniaxial tension-compression low cycle fatigue method. The experimental results indicate that the internal fatigue micro-crack clearly evolves from the original penny-shaped crack into a string of spherical voids in the longitudinal section plane of the fatigue sample after the vacuum diffusive healing at the high temperature. The quantitative relationship between the radius and the spacing of spherical voids depends on the crack position (within grains, on grain boundaries or transgranular sites) and its orientations within the grain. The diffusive healing, the related thermodynamics and mechanism, and the effect of the surface tension anisotropy on the relationship between void diameter and void spacing are also discussed.

[Key words] pure titanium; internal fatigue micro-crack; diffusive healing
[CLC number] TG111.6; TG111.8 [Document code] A

1 INTRODUCTION

Titanium and its alloys with particular properties are widely used in many industry fields. They unavoidably undergo various damages in service. The nucleation and growth of internal fatigue micro-cracks have deleterious effects on the strength and toughness of the alloys. High temperature healing of the internal fatigue micro-cracks can cause partial or complete recovery of mechanical properties, and ensure the reliability of the structures with the low cost.

There was much investigation on internal crack healing over the past 40 years[1~12], most of which was focused on the morphology evolution of the internal crack, particularly its mechanism. Based on the investigation on the infinite long liquid cylinder[13], the morphology stability of many materials was studied with the perturb method[14~19]. From the dynamic point, all factors related to the diffusion behavior will affect the crack healing process. As the initial boundary condition of the atom diffusion, the shape and size of cracks have dominant effects on its morphology evolution during the healing.

Up to now, the major investigation of the crack healing was focused on the porous materials such as cracked ceramics. In this paper, the investigation is performed on the internal micro-crack healing behavior of the commercial pure titanium.

2 EXPERIMENTAL

The test material is commercial pure titanium TA_2 with a purity of 99%. After the cold extrusion the materials was annealed at 750 ±10 ℃ for 3 h. The recrystallized grains were equiaxed with the average size about 30 μm. The yield strength of the material is 350 MPa; the fracture strength is 475 MPa, and the reduction in area is about 55%.

Low cyclic fatigue tests were performed in MTS880 machine, and were carried out under an uniaxial symmetric tension-compression load with a cyclic frequency of 0.5 Hz and a sine wave at 298 K. The load direction was parallel to the symmetric axis of the specimen.

The healing treatment was carried out by a vacuum diffusive annealing under vacuum of 10^{-2} Pa at 1 200 ℃ for 2 h. The crack morphology was observed by means of the scanning electron microscopy (SEM), and the observed plane was the side (longitudinal) section parallel to the symmetric axis of the specimen.

3 EXPERIMENTAL RESULTS

Fig. 1 shows the fatigue life (N_f) in the low cyclic deformation at the strain ranges ($\Delta\varepsilon/2$) from 4×10^{-3} to 1.5×10^{-2} at room temperature. The Manson-Coffin relationship is given by

$$(\Delta\varepsilon/2)N_f^{0.281}=0.056 \quad (1)$$

Fig. 2 shows the low cyclic fatigue cracks located on the longitudinal section parallel to the load direction in the pure titanium sample, observed by SEM. It indicates that the fatigue cracks mostly locate at the

① [Foundation item] Project (59925104) supported by the National Outstanding Young Investigator Grant of China; Project (59889101) supported by the National Natural Science Foundation of China [Received date] 2001- 03- 05; [Accepted date] 2001- 06- 04

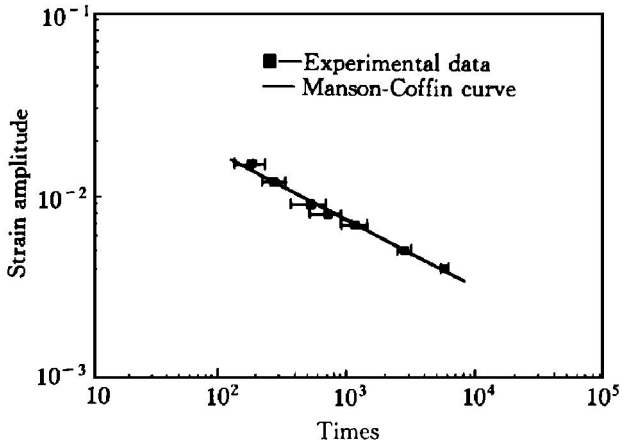

Fig. 1 Fatigue life in low cyclic deformation and Manson-Coffin curve for pure titanium

Fig. 2 Fatigue crack located on longitudinal section of pure titanium sample

sub-surface or penetrate to the surface of the samples with the length of millimeters and the width more than 1 μm. With increasing the cyclic strain, the amount of the fatigue cracks increases and the ratio of the internal crack number to the total of fatigue cracks increases too. Fig. 3 shows the representative internal fatigue crack that is almost a beeline in two-dimension and a penny-shaped in three-dimension, with the critical length about 30 μm and the width less than 1 μm.

Fig. 4 shows several internal micro-cracks observed by SEM on the longitudinal section plane of the sample after vacuum annealing. It indicates that the internal fatigue micro-crack is clearly evolved from the original penny-shape to a string of spherical voids. Moreover, the ratio of the spacing to the diameter of the void with the similar orientations in one grain are similar to each other. And the ratio of the spacing to the diameter of the void with different orientation in one grain is not clearly the same. The ratio of the spacing to the diameter of the void in the grain are clearly different from that in the neighboring grain. Same condition occurs on the grain boundaries compared with that within grains.

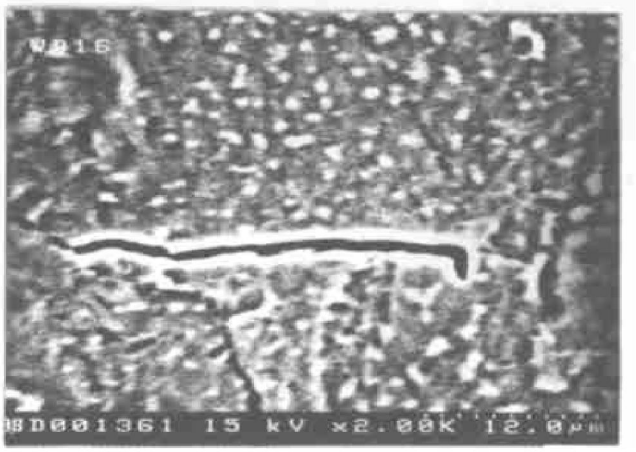

Fig. 3 Two-dimensional morphology of internal fatigue micro-crack on longitudinal section of pure titanium sample

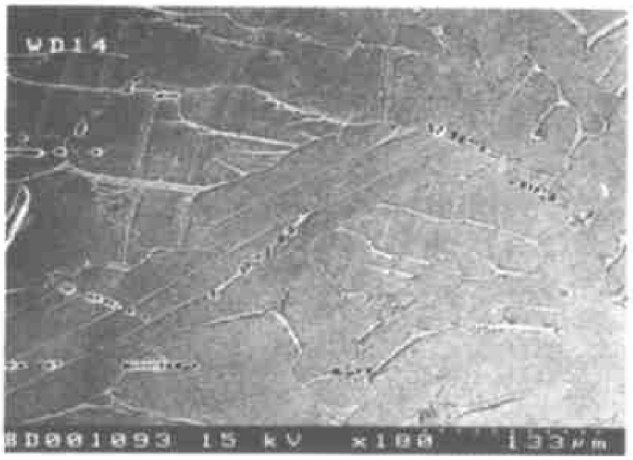

Fig. 4 Two-dimensional morphology of spherical voids after vacuum annealing

Fig. 5 shows the representative morphologies of four internal micro-cracks observed on longitudinal section by SEM after annealing. In Fig. 5(a), the right part of the internal micro-crack is evolved into three spherical voids, and the diameter of spherical void near the crack tip is the smallest. The left tip is broken to one spherical void, and symmetrical concave and convex are formed in the middle part. In Fig. 5(b), three spherical voids are formed in the middle part of the internal micro-crack; the left tip is broken to one spherical; and the symmetrical concave and convex are formed in the right. In Fig. 5(c), the right part of the main crack entirely evolves into a string of spherical voids, and the second crack also evolves into an array of spherical voids, but the spacing of the voids from the second crack is clearly larger than that from the main crack. In Fig. 5(d), the whole crack entirely evolves into spherical voids, and the void diameter in the middle is bigger than those at crack tips, which will entirely vanish after continuous shrinkage with increasing the time of annealing.

Fig. 6 shows the change of spacing with the dia-

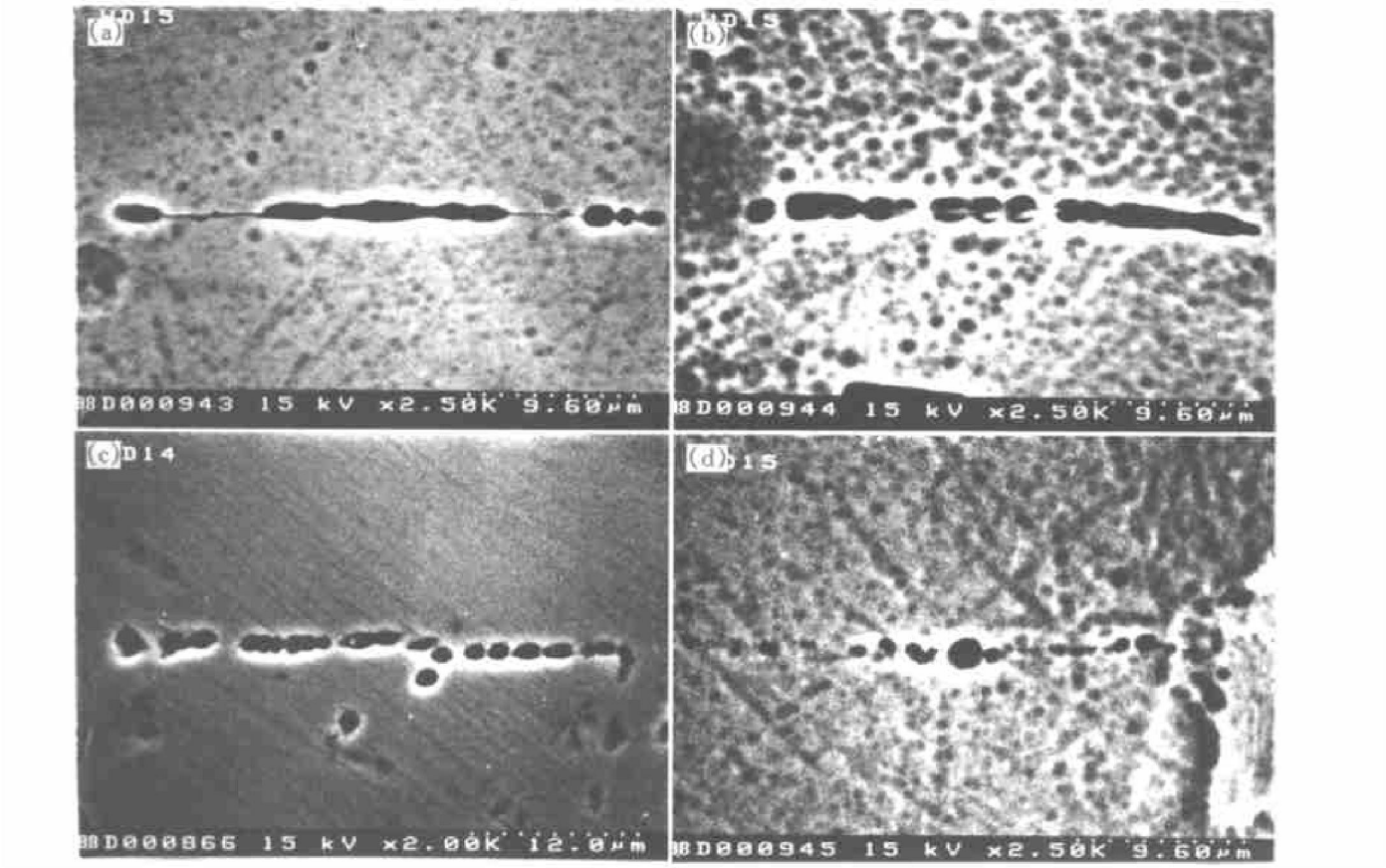

Fig. 5 Typical morphologies of fatigue cracks after vacuum annealing

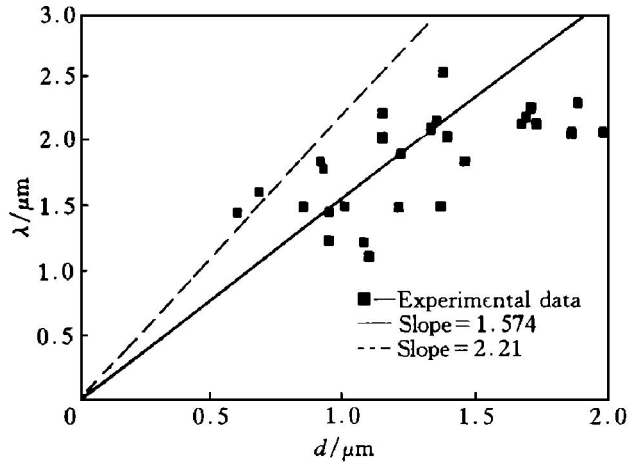

Fig. 6 Spacing vs diameter of spherical voids in longitudinal section plane

meter of spherical voids measured in the Fig. 5. The void diameter ranges from 0.46 μm to 1.97 μm, and the void spacing ranges from 1.1 μm to 2.54 μm with the ratio of diameter to spacing from 1.1 to 2.48 and the average of 1.574. It is noted that the void morphologies observed in the Figs. 4 and 5 are two-dimensional in any longitudinal section plane of the crack. On the viewpoint of the geometry, the void diameter on two-dimensional section plane is less and its average is $0.785\pi/4$ times the real size of the three-dimensional one. The void spacing on two-dimensional section plane is less and its average is $(d/\lambda)/\arcsin(d/\lambda)$ times the real size of the three-dimensional one (where d is the void diameter and λ is the spacing). When prepare the samples, the surface of voids can be corroded on etching sample so that the void diameter is more than the real size on the two-dimension, but the void spacing is not changed.

4 DISCUSSION

4.1 Evolution mechanism of internal micro-cracks by diffusive healing

On the surface of the internal fatigue micro-cracks of pure titanium sample, the chemical potential per atom (μ_K) is given by[22]

$$\mu_K = \mu_0 \pm \Omega\gamma K \qquad (2)$$

where K ($K = K_1 + K_2$) is the total curvature and its value is always positive. K_1 and K_2 are two principal curvatures of the crack surface, μ_0 is the chemical potential per atom on the flat surface, γ is the surface tension (assumed isotropic here) and Ω is the atomic volume. The minus sign represents the concave surface and the positive sign represents the convex surface.

The curvatures are clearly different at the various point of the penny-shaped crack surface so that it will cause the difference on the chemical potential per atom on the crack surface. The gradient of atoms chemical potential becomes the driving force of atom diffusion along the crack surface. The titanium atoms

diffuse to the edges of the penny-shaped crack because the surface curvature at the edges is bigger than that at the other points. The edges of the crack recede toward the center and the crack surface moves along the normal moving direction. The normal velocity of the crack surface is given by[22]

$$\frac{\partial n}{\partial t} = B_S \nabla_S^2 K \quad (3)$$

where $B_S = D_S \upsilon K / kT$, $\nabla_S^2 K$ is surface laplacian of K, D_S is the surface atoms self-diffusion coefficient (assumed isotropic), υ is the number of diffusing atoms per unit surface area, k is Boltzman's constant and T is the healing temperature. Therefore, under the initial condition and boundary condition of the atom diffusion, the crack surface will move on the rule described in the Eqn. (3), and the crack is replaced by a cluster of channel pores with a sphere in the center.

All the channel pores are still unstable thermodynamically and will continue to evolve because of the longitudinal perturbation (titanium atom surface self-diffusion). It can be thought that this evolution of the channel pores is similar to that of an infinite long cylinder that evolves into an array of spherical voids. The transformation from the penny-shaped crack to a lot of spherical voids results in a net reduction in total interfacial energy of the system even when the total volume of voids space remains constant. The atom self-diffusion does not occur on the spherical void because the curvatures at every point are the same. However, the spherical void will vanish after continuous shrinkage by the atom self-diffusion from the crystal to the void surface.

From above, the process of morphology evolution can be divided into three stages and the mechanism is shown in Fig. 7. At first, the edges of the crack recede toward the center, and the penny-shaped crack will evolve into a cluster of channel pores. Then these channel pores break into an array of the spherical voids with a spherical void in the center. Finally, the spherical voids will vanish after continuous shrinkage. It should be emphasized that these stages could overlap each other due to the difference in the size and the morphology of the cracks.

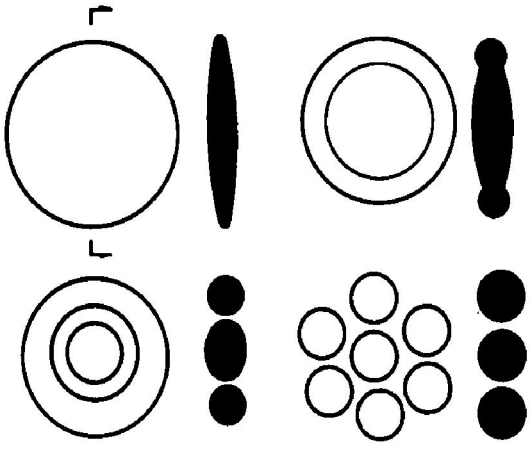

Fig. 7 Schematic representation of evolution mechanism of ellipsoidal crack

4.2 Change of system free energy during healing

In the first two evolution stages, the total volume of voids remains constant. The system free energy change ΔG is equal to the total surface energy change, as given by

$$\Delta G = \gamma (S - S_0) \quad (4)$$

where S_0 is the initial area of internal micro-crack surface and S is the surface area of total spherical voids after healing. If the internal penny-shaped micro-crack is regarded as the ellipsoidal crack with the diameter of L and the crack thickness of h, the ratio of the diameter to the thickness of a crack (L/h) is β. Assuming n spherical voids evolve from ellipsoidal cracks with the same diameter and various β, the surface energy can be expressed by

$$\Delta G = \pi \gamma h^2 \left\{ \beta^{4/3} n^{1/3} - \frac{1}{2} \left[\beta^2 + \sqrt{\frac{\beta^2}{\beta^2 + 1}} \cdot \ln\left(\beta + \sqrt{\beta^2 - 1} \right) \right] \right\} \quad (5)$$

Fig. 8 shows the free energy changes $\Delta G / \pi \gamma h^2$ as function of β and the total number of spherical voids respectively. If β is bigger than β_{min} for ellipsoidal cracks breaking up into the equivalent number

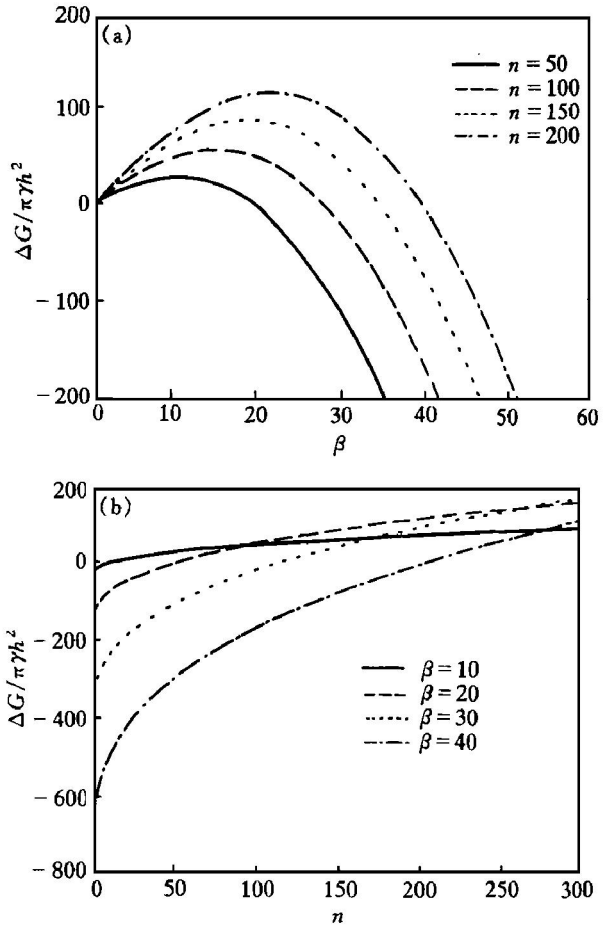

Fig. 8 Free energy changes as function of β and n
(a) $-\Delta G / \pi \gamma h^2$ vs β; (b) $-\Delta G / \pi \gamma h^2$ vs n

of voids, or the total number of spherical voids is smaller than n_{max}, the system free energy changes are always negative. In another word, the system free energy always decreases for the appropriate size of the internal micro-crack to evolve into voids. It is easy to satisfy the above condition for the low cyclic fatigue micro-cracks of the pure titanium, so they can be broken into spontaneously spherical voids by the vacuum annealing.

If we regard the internal micro-crack with the penny-shaped as the plate-shaped, the free energy change is similar to the ellipsoidal crack. But the number of spherical voids evolved from two shape cracks is different with each other. Fig. 9 shows the changes in n_{max} (maximum number of the spherical void from the plate-shaped crack) and d_{min}/h (the ratio of the minimum diameter of the spherical void to the thickness) of the plate-shape as function of β respectively. The calculation results indicate that the maximum number of voids evolved from the ellipsoidal crack is more than that from the plate-shaped crack and the minimum diameter of the void evolved from the ellipsoidal crack is smaller than that from the plate-shaped crack with the same β. Moreover, the diameter of voids from both of two shaped cracks is always bigger than the original crack thickness, and is two and three times the thickness of two shaped cracks, respectively.

At the third stage, because the volume of spherical void and the surface area of the spherical void decrease, the titanium atom chemical potential at the crack surface and the system free energy always reduce during the void shrinking, which can be predicted that this process is spontaneous.

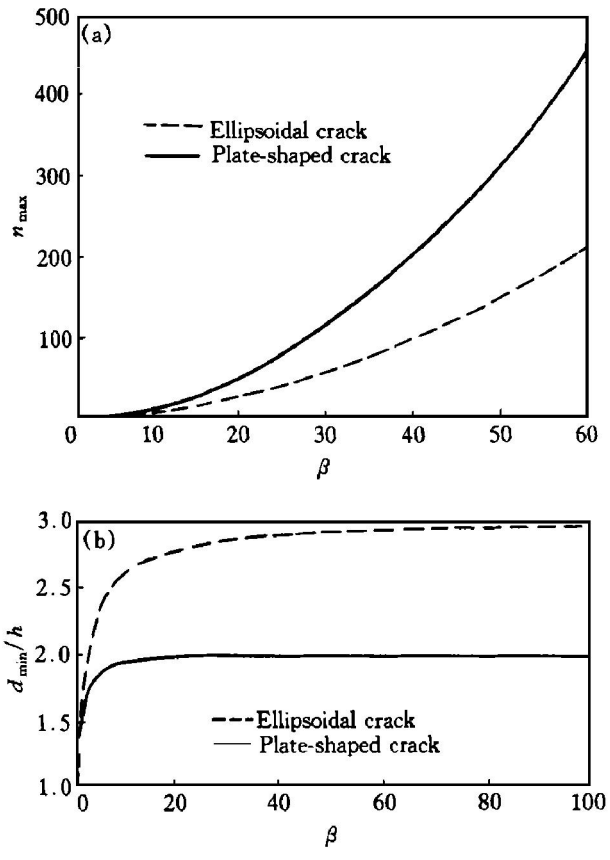

Fig. 9 Changes in n_{max} and d_{min}/h as function of β
(a) —n_{max} vs β; (b) —d_{max}/h vs β

4.3 Effect of surface tension anisotropy on relationship between void diameter and spacing

The diameter and the spacing are two main parameters that represent the characteristics of the spherical voids evolved from the internal micro-cracks. The ratio of the diameter to the spacing of the spherical voids is not the same for the different evolution stage. Considering the surface tension isotropy, a longitudinal perturbation with wavelength bigger than the minimum wavelength λ_{min} ($2\pi R$) will spontaneously increase in amplitude for a infinite cylinder with the radius of R because the system free energy is reduced, and so a unstable cylinder will evolve into a line of spheres with increasing time. For a longitudinal perturbation with wavelength of λ_m, the velocity in amplitude is the maximum, so the infinite cylinder finally break up into an array of spheres with the spacing λ_m and the radius r. The dominant diffusion path can be identified by the ratio of the spacing to the radius or the diameter of sphere. When the surface atoms self-diffusion is dominant, $\lambda_m/R = 8.89$, and $\lambda_m/r = 4.73$; and when the lattice atoms self-diffusion is dominate, $\lambda_m/R = 12.96$, and $\lambda_m/r = 6.07$[9, 15]. For bubbles formed within a grain, the spacing would be $\lambda_m = 2.43d$ controlling by surface diffusion and $\lambda_m = 2.94d$ by lattice diffusion[23]. The finite cylinder with two hemispherical ends would transform into two or more isolated pores when the ratio of cylinder length to diameter was greater than 7.2[16]. In this case, the spacing in terms of the final pore size would be $\lambda_m = 4.41r$ controlling by surface diffusion[9].

However, the surface tension is actually anisotropic on the crystal surface and so the surface tension of the infinite cylinder void is expressed by

$$\gamma(\theta) = \gamma_0(1 - \alpha\theta^2) \quad (5)$$

where γ_0 is the surface tension at the circular cross-section of the cylinder, θ is the angle of the normal vector of the arbitrary surface from that of the circular cross-section of the cylinder after the shape is changed and α is a dimensionless number to indicate the anisotropy. In this case, the minimum wavelength λ_{min} will change from $2\pi R$ to $2\pi R\sqrt{1-2\alpha}$.

The calculation result indicates that λ_{min} reduces with increasing α, λ_{min} may be more than $2\pi R$ at $\alpha < 0$ or less than $2\pi R$ at $\alpha > 0$. The spacing, the diameter and their ratio of voids from the cylinder reduce with increasing α. The cylinder is unstable for perturbation of any wavelength if the surface tension is very anisotropic, i.e., $\alpha > 1/2$. Thus, the quanti-

tative relationships between the radius and the spacing of spherical voids depend strongly on the surface tension anisotropy.

In the Figs. 4 and 5, assuming the lattice diffusion also exists, the ratio of the spacing to the diameter of spherical voids that form at the second or the third stage of the evolution, is more than 2.21. However, Experimental results show that the ratio depends on the crack position (within grains, on grain boundaries or transgranular sites) and its orientations within the grain. In fact, most are near or less than 2.21 and much scattered.

5 CONCLUSIONS

1) The two-dimensional internal fatigue microcrack is clearly evolved from the original penny-shaped crack into a string of spherical voids in the longitudinal section plane after the vacuum diffusive healing at the high temperature.

2) The evolution consists of three stages. At first, the edges of the crack recede toward the center, and the penny-shaped crack evolves into channel pores. Then these channel pores break into strings of the spherical voids with a spherical void in the center. Finally, the spherical voids vanish after continuous shrinkage.

3) The surface energy anisotropy can affect the relationship between void diameter and void spacing. And the quantitative relationships between the radius and the spacing of spherical voids depends on the crack position (within grains, on grain boundaries or transgranular sites) and its orientations within the grain.

[REFERENCES]

[1] Lange F F, Gupta T K. Crack healing by heat treatment [J]. J Am Ceram Soc, 1970, 53(1): 54- 55.

[2] Bandyopadhyay G, Roberts J T A. Crack healing and strength recovery in UO_2[J]. J Am Ceram Soc, 1976, 59(9- 10): 259- 262.

[3] Evens A G, Charles E A. Strength recovery by diffusive crack healing [J]. Acta Met, 1977, 25: 919.

[4] Smith D L, Evans B. Diffusional crack healing in quartz [J]. J Geophysical Research, 1984, 89: 4125- 4135.

[5] Gupte T K. Crack healing in thermally shocked MgO [J]. J Am Ceram Soc, 1975, 58: 143.

[6] Gupte T K. Kinetics of strengthening of thermally shocked MgO [J]. J Am Ceram Soc, 1976, 59: 259.

[7] Gupte T K. Instability of cylindrical voids in alumina [J]. J Am Ceramic Soc, 1978, 61: 191- 195.

[8] Gupte T K. Crack healing in Al_2O_3, MgO, and related materials [J]. Adv Ceram, 1984, 10: 750- 766.

[9] Yen C F, Coble R L. Spheroidization of tubular voids in Al_2O_3 in high temperature [J]. J Am Ceram Soc, 1972, 55: 507- 509.

[10] Dutton R. Comment on "Crack Healing in UO_2" [J]. J Am Ceram Soc, 1973, 56: 660- 661.

[11] Power J D, Glaesr A M. Higlr-temperature healing of cracklike flaws in Mg- and Ca-ion-implanted sapphire [J]. J Am Ceram Soc, 1992, 75(9): 2547- 2558.

[12] Harold D Ackler. Healing of lithographically introduced cracks in glass and glass-containing ceramics [J]. J Am Ceram Soc, 1998, 81: 3093- 3103.

[13] Rayleigh L. On the instability of jets [J]. London Math Soc Proc, 1878, 10: 4.

[14] Nichols F A, Mullins W W. Morphological changes of a surface of revolution due to capillarity-induced surface diffusion [J]. J Appl Phys, 1965, 36: 1826- 1835.

[15] Nichols F A, Mullins W W. Surface-(interface-) and volume-diffusion contributions to morphological changes driven by capillarity [J]. Transaction of the Metallurgical Society of AIME, 1965, 233: 1840- 1847.

[16] Nichols F A. On the spheroidization of rod-shaped particles of finite length [J]. J Met Sci, 1976, 11: 1077.

[17] YANG Lai-tian, Wayne K R. Mechanisms of pearlite spheroidization [J]. Metallurgical Transactions A, 1987, 18A: 1403- 1414.

[18] Carter W C, Glaeser A M. The effect of finite amplitude perturbations on the stability of continuous phases [J]. Mater Sci Eng, 1987, 89: L41- L45.

[19] Briant C L. Potassium bubbles in tungsten wire [J]. Metallurgical Transaction A, 1993, 24A: 1073- 1084.

[20] Mullins W W. Mass transport at interfaces in single component systems [J]. Metallurgical and Materials Transactions A, 1995, 26A: 1917- 1929.

[21] Mishin Y, Herzig C. Diffusion in the Ti-Al system [J]. Acta Mater, 2000, 48: 595.

[22] Herring H. Physics of Powder Metallurgy [M]. New York: McGraw-Hill, 1951: 143.

[23] Moon D M, Koo R C. Mechanism and kinetics of bubble formation in doped tungsten [J]. Metallurgical Transaction, 1971, 2: 2115- 2122.

[24] Suo Z. Motions of microscopic surfaces in materials [J]. Advances in Applied Mechanics, 1997, 23: 249.

(Edited by YANG Bing)